Reduced mesophyll conductance by cell wall thickening and chloroplasts decreasing driven the decline of photosynthesis under sole NH_4^+ supply

Yiwen Cao, Yonghui Pan, Tianheng Liu, Min Wang, Shiwei Guo*

Jiangsu Provincial Key Lab for Organic Solid Waste Utilization; National Engineering Research Center for Organic-based Fertilizers; Jiangsu Collaborative Innovation Center for Solid Organic Waste Resource Utilization; Nanjing Agricultural University, Weigang 1, Nanjing 210095, China

* Corresponding author: E-mail, sguo@njau.edu.cn; Fax, +86-25-84396393

Yiwen Cao: 2020203071@stu.njau.edu.cn

Yonghui Pan: pyh2014@webmail.hzau.edu.cn

Tianheng Liu: 2020803194@stu.njau.edu.cn

Min Wang: minwang@njau.edu.cn

Shiwei Guo: sguo@njau.edu.cn

The date of submission: 5 January 2022

The number of tables and figures: 3 and 6, respectively

Word count: 3554

Highlight: Cell wall and chloroplast variability determining the mesophyll conductance under different nitrogen forms

Abstract: The relationship between nitrogen (N) sources and photosynthetic capacity of leaf differs between species. However, the leaf anatomical variabilities related to photosynthesis (*A*) of shrubs under different forms of N remain imperfectly known. Here, *Lonicera Japonica* (a shrub) was grown hydroponically in the presence of three forms of N (sole NH_4^+, 50%/50% NH_4^+/NO_3^- and sole NO_3^-). *A* and photosynthetic N use efficiency significantly decreased under sole NH_4^+ supply, in parallel with down-regulated stomatal conductance (g_s), mesophyll conductance (g_m), and electron transfer rate (J). Up to the total *A* decline of 41.28% in sole NH_4^+ supply (compare with sole NO_3^-), the g_m attributed to 60.3% of the total limitations. Besides, the decreased internal air space explained the increase of gas-phase resistance, and the increased liquid-phase resistance in sole NH_4^+ supply was ascribed to the thicker cell wall thickness (T_{cw}) and decreased chloroplasts exposed surface area per unit leaf area (S_c/S). The discrepancy of S_c/S could be interpreted by the altered chloroplasts numbers and the distance between adjacent chloroplasts ($D_{chl\text{-}chl}$). These results indicate the alteration of T_{cw} and chloroplast numbers were the main causes of the difference in g_m in coping with varied N sources.

Key words: Ammonium; leaf anatomy; *Lonicera Japonica*; mesophyll conductance; N form; nitrate; photosynthetic limitations; shrub

Introduction

Lonicera Japonica is a widespread semi-deciduous shrub species of the Caprifoliaceae family utilized in traditional medical practices (Schierenbeck, 2004; Shang *et al.*, 2011). The stomatal and photosynthetic function are suggested the key traits for enhancing yield and quality of medicinal plants, as the photosynthesis improvement could increase carbon fixation and the production of biomaterials. Mesophyll conductance (g_m) represents the diffusion conductance to CO_2 in the mesophyll tissues from the sub-stomatal cavities to the carboxylation sites inside chloroplast (Peguero-Pina *et al.*, 2012), which was proposed to be the first limiting factor in photosynthesis (Lu *et al.*, 2016; Ren *et al.*, 2019).

g_m is determined by the CO_2 diffusion characteristic. CO_2 diffusion, according to Fick's law, depends on CO_2 diffusivity, leaf temperature, diffusion distance, and the nature of the media in which diffusion occurs (e.g., mesophyll tissues) (Flexas *et al.*, 2012), thus it is not strange that even tiny leaf anatomical traits could drive g_m variability. Tholen *et al.* (2012a) had reported that altered leaf anatomy significantly influences the CO_2 diffusion in leaves. Leaf mass per area (M_A) is an important integrated leaf morphological characteristic that regulates photosynthesis by influencing g_m (Niinemets, 2001; Poorter *et al.*, 2009). Early studies reported a negative correlation between M_A and g_m (Flexas *et al.*, 2008; Niinemets *et al.*, 2009b), and further in species with high M_A, photosynthesis is more limited by g_m, on average by 57% (Tomás *et al.*, 2013); analyses on the relationship between g_m and leaf density/leaf thickness, two components of M_A also corroborated this idea, despite the influences are opposite. The increase of M_A due to increased leaf density might result in a densely packed mesophyll cell, which will ultimately reduce the g_m by decreased mesophyll surface area exposed to intercellular airspace per unit leaf area (S_{mes}/S) (Flexas *et al.*, 2008; M. Weraduwage *et al.*, 2016).

In the journey of CO_2 diffusion, the mesophyll resistance is comprised of gas-phase resistance (i.e., from the intercellular air space) and liquid-phase resistance

(i.e., from the cell wall, lipid membrane, cytoplasm, stroma, and chloroplast envelope). In particular, liquid-phase limitation accounts for more than 80% of the total limitation, in which the cell wall thickness (T_{cw}) and chloroplast surface area exposed to intercellular airspace per unit leaf area (S_c/S) are the two dominating components that affect g_m (Flexas *et al.*, 2021). There are ample studies showing a significant positive correlation between S_c/S and g_m, and the S_c/S was considered the uppermost parameter in determining g_m (Hu *et al.*, 2020; Tomás *et al.*, 2013). While the cell wall is often negligible, because it accounts for a tiny fraction of the CO_2 diffusion length (Carriquí *et al.*, 2020), has a comparative larger pore size and variability (Carpita *et al.*, 1979), and quite a static influence on photosynthesis (Evans *et al.*, 2009). Interestingly, in *Lycopodiales* (a species of fern), the accountability of T_{cw} in robust leaves of the total g_m was up to 70% (Tosens *et al.*, 2016). Other components, such as the mesophyll thickness, plasma membrane, and chloroplast density, despite not that important, also play an important role in regulating g_m, as observed in different plant species (Lu *et al.*, 2016; Niinemets *et al.*, 2009b; Veromann-Jurgenson *et al.*, 2020a; Veromann-Jurgenson *et al.*, 2020b). Overall, the leaf anatomies might vary independently and compensate for each other to achieve substantial g_m in some cases (Peguero-Pina *et al.*, 2017).

In fact, g_m is a rapidly adapting trait, and thus its value presents a large variability across species or environments. Up to now, mesophyll conductance to CO_2 had been studied on various plant species in a scale of interspecific variation and diverse environmental conditions. The review of Flexas *et al*. (2008) summarized the g_m in different pooled groups of plants, which showed an apparent increasing tendency of g_m from conifers (slightly above 0.1 mol m^{-2} s^{-1}) to grasses (0.2-0.4 mol m^{-2} s^{-1}), and the semi-deciduous shrubs generally had a g_m value of 0.2-0.3 mol m^{-2} s^{-1}. The varying environmental conditions, such as light, water availability, salinity, and temperature had also been studied in regulating g_m (Flexas *et al.*, 2008; Niinemets *et al.*, 2009b; Pons *et al.*, 2009; Tosens *et al.*, 2012a). In contrast, the effects of nutrition

on g_m, particularly on quantitative limitations of g_m are somewhat incomplete, and only recently have the effects of nutrition (e.g., potassium, nitrogen) been reported (Gao *et al.*, 2020; Hu *et al.*, 2020; Xie *et al.*, 2020; Xiong *et al.*, 2015b). Nitrogen (N) is an important nutrition element for plant growth and photosynthesis. There is sufficient evidence of the strong interplays between the photosynthetic process and plant endogenous N status (Perchlik and Tegeder, 2018; Xiong *et al.*, 2015). N in soil is available mainly in two inorganic N sources, i.e., nitrate (NO_3^--N) and ammonium (NH_4^+-N). Due to the different assimilation processes and energy consumption, or sometimes the toxic effect of NH_4^+, photosynthesis of species showed quite different responses/preferences to NH_4^+ or NO_3^-. In some studies, the plant supplied with NH_4^+ was observed increased chloroplast numbers and chloroplast volume in comparison with NO_3^- (Golvano *et al.*, 1982), yet the other study observed an elevated S_c/Rubisco in NO_3^- supply (Gao *et al.*, 2020); this effect on photosynthetic capacity and g_m, according to some studies, could be ascribed to N allocation trade-off and source-sink balance within leaves (Evans and Clarke, 2019; Hikosaka, 2004). The studies on the relative importance of N source to the response of g_m variation in a scale of leaf structural traits had been reported in herbs (Gao *et al.*, 2020) and trees (Liu *et al.*, 2021), while the study on shrubs is largely lost. Moreover, major limiting factors that restrict the leaf photosynthetic capacity of *L. Japonica* under different inorganic source is largely unknown.

In the present study, *L.Japonica* was grown in a hydroponic experiment with three forms of N (sole NH_4^+, 50%/50% NH_4^+/NO_3^- and sole NO_3^-) to investigate: (1) the variations of leaf photosynthesis and leaf anatomy under different inorganic nitrogen sources; (2) the crucial role of g_m on leaf photosynthesis of *L. Japonica*; (3) the impact of mesophyll conductance on leaf photosynthesis through leaf structure variations.

Material and Methods

Plant material and experimental condition

The hydroponic experiment was conducted in a greenhouse with a light intensity of 1000 μmol photons m^{-2} s^{-1} at the leaf level using 14-h photoperiod and day/night temperature of 28/18□. The experimental site is located in Nanjing (118°51'E, 32°1'N), China. One-year-old seedlings of *Lonicera japonica* were transferred to a 12 L rectangular plastic box (64 cm×23 cm×18 cm) and a one-half-strength mixture of NH_4^+ and NO_3^- nutrient solution was supplied (for composition, see below). After two weeks, the seedlings were supplied with full-strength nutrition solution for two weeks, after which the uniform seedlings were transplanted to a 12 L rectangular plastic box (64 cm×23 cm×18 cm). The nutrition solution contained 2.0 mM $MgSO_4 \cdot 7H_2O$, 2.8 mM $CaCl_2 \cdot 2H_2O$, 1.03 mM K_2SO_4, 0.32 mM KH_2PO_4, 9.10×10^{-3} mM $MnCl_2 \cdot 4H_2O$, 0.52×10^{-3} mM $(NH_4)_6Mo_7O_{24} \cdot 4H_2O$, 37×10^{-3} mM H_3BO_3, 0.15 $\times10^{-3}$ mM $ZnSO_4 \cdot 7H_2O$, 0.16 $\times10^{-3}$ mM $CuSO_4 \cdot 5H_2O$, 35.8×10^{-3} mM Fe-EDTA. In our preliminary experiment, plant growth was highest at a ratio of 50%/50% NH_4^+/NO_3^- compared with 75%/25% NH_4^+/NO_3^- and 25%/75% NH_4^+/NO_3^- at a N level of 2.8 mM. Thus, the N was supplied at 2.8 mM with three different treatments: sole $(NH_4)_2SO_4$ (A), sole Ca $(NO_3)_2$ (N) or mixed N (combination of 50% $(NH_4)_2SO_4$ and 50% Ca $(NO_3)_2$, AN). $CaCl_2$ was added to the solutions of A and AN treatment to adjust the Ca level to N treatment (2.8 mM). Dicyandiamide was added to each nutrition solution as nitrification inhibitor. The nutrition solution was aerated for 1-h/1-h day/night and renewed every 4 days, while the pH was adjusted to 6.0±0.1 each day. The containers were placed randomly to prevent the position effect.

Gas exchange and chlorophyll fluorescence measurement

Leaf gas exchange and chlorophyll fluorescence were measured simultaneously using an open gas exchange system equipped with multiphase flash (LI-6800XT; LI-COR Inc., Lincoln, NE, USA) from 8:30 to15:00. For each treatment, new fully-expanded leaves were randomly selected for the measurements with five replications. Measurements were obtained at a leaf temperature of 28±0.5°C, CO_2 concentration inside the chamber of 400±6 μmol mol^{-1}, and a photosynthetic photon

flux density (PPFD) of 1000 μmol photons m^{-2} s^{-1}. For fluorescence parameters, steady-state fluorescence yield (F_s) and maximum fluorescence (F_m') were recorded using a fluorometer chamber during a light-saturating pulse of approximately 8000 μmol m^{-2} s^{-1}. During the photosynthetic CO_2 responses (A/C_i curve) measurements, the ambient CO_2 concentration (C_a) was set in a series from 400 to 300, 200, 150, 100, and 50 μmol CO_2 mol^{-1} and then increased from 50 to 400, 600, 800, and 1000 μmol CO_2 mol^{-1} at a constant PPFD of 1000 μmol m^{-2} s^{-1} with four replicates. The maximum carboxylation rate (V_{cmax}) was calculated according to Long and Bernacchi (2003), and the carboxylation efficiency (*CE*) was estimated as the slope of the A/C_i curve fitting line over a C_i range of 50-200 μmol mol^{-1}. The effective quantum efficiency of photosystem II (ΦPSII) was quantified as follows: $\Phi PSII=(F_m'-F_s)/F_m'$. The potential electron transport rate (J) was calculated as $J= \Phi PSII \times PPFD \times \alpha \times \beta$, where α is the leaf absorption and β is the proportion of quanta absorbed by PSII, assumed as 0.85 and 0.5, respectively. There were no differences in chlorophyll contents between A, N, and AN leaf, thus eliminating out the confounding effect of different leaf optical properties as a result of N forms among the treatments.

Then we estimated the mesophyll conductance (g_m) and chloroplast CO_2 concentration (C_c) by variable J method proposed by Harley *et al*. (1992).

$$g_m = \frac{A}{C_i - \frac{\Gamma^*(J+8(A+R_d))}{J-4(A+R_d)}} \quad (1)$$

$$C_c = C_i - \frac{A}{g_m} \quad (2)$$

where A, C_i, C_c, and J were calculated as described previously, $\Gamma^*$is the CO_2 compensation point in the absence of mitochondrial respiration and R_d is the mitochondrial respiration rate in the light. In this study, $\Gamma^*$was assumed to be 40.0 μmol m^{-2} s^{-1}, and R_d, according to the previous data, was assumed to be 1.0 μmol m^{-2} s^{-1}.

Leaf physiology

Four new fully expanded leaves from each treatment were randomly selected and

pictured. The leaf area (A_L) obtained from the picture was calculated by Image-Pro Plus (Media Cybernetics, Sliver Spring, MD, USA), after which the leaves were oven-dried at 105°C for 15 min and then dried to constant weight at 65°C and weighted. Dried leaf samples were weighed and digested with H_2SO_4-H_2O_2 at 270 °C, and the leaf N concentration was determined using the digital colorimeter (AutoAnalyzer 3; Bran+Luebbe). The total chlorophyll concentration was determined according to the method proposed by Sartory and Grobbelaar (1984). Approximately 0.5 g fresh leaf discs (avoiding the main vein) were extracted with 50 ml 95%(v/v) ethanol (analytically pure, Sinopharm Chemical Reagent Co., Ltd) in the dark until they were blanched (usually no more than two days). The extract solutions were used for the determination of chlorophyll *a* and *b* using a spectrophotometer (HBS-1096A, Shanghai, China) at 665 and 649 nm, respectively. The total chlorophyll was calculated as the sum of chlorophyll *a* and *b*. There were four replications for chlorophyll concentration determination.

Quantitative limitation analysis of *A*

To separate the relative controls on *A* resulting from the difference in stomatal conductance, mesophyll diffusion, and biochemical capacity, quantitative analysis was conducted. The limitation of *A* under different types of N forms, according to Grass and Magnani (2005), was then composed of stomatal limitation (S_L), mesophyll conductance (MC_L), and biochemical limitation (B_L), which could be expressed as follows:

$$\frac{dA}{A} = l_s * \frac{dg_s}{g_s} + l_m * \frac{dg_m}{g_m} + l_b * \frac{dJ}{J} \quad (3)$$

where the l_s, l_m, and l_b ($l_s+l_m+l_b=1$) were the relative limitation of stomatal conductance, mesophyll diffusion and biochemical capacity, which were calculated as follows:

$$l_s = \frac{g_{tot}/g_s * \partial A/\partial C_C}{g_{tot} + \partial A/\partial C_C} \quad (4)$$

$$l_m = \frac{g_{tot}/g_m * \partial A/\partial C_C}{g_{tot} + \partial A/\partial C_C} \quad (5)$$

$$l_b = \frac{g_{tot}}{g_{tot} + \partial A/\partial C_C} \quad (6)$$

where the g_{total} is the total conductance to diffuse CO_2 from the leaf surface (i.e., inside the leaf boundary layer) to the carboxylation site of chloroplast, which can be calculated as $\frac{1}{g_{tot}} = \frac{1}{g_s} + \frac{1}{g_m}$. $\partial A/\partial C_c$ was estimated as the slope of A/C_i curves over a C_i range of 50-100 μmol mol^{-1}.

Then, the limitations of A can be approximately calculated as follows:

$$S_L = l_s * \frac{g_{sref} - g_s}{g_{sref}} * 100 \quad (7)$$

$$MC_L = l_m * \frac{g_{mref} - g_m}{g_{mref}} * 100 \quad (8)$$

$$B_L = l_b * \frac{J_{ref} - J}{J_{ref}} * 100 \quad (9)$$

where g_{sref}, g_{mref}, and J_{ref} are the reference values of stomatal conductance (g_s), mesophyll conductance (g_m), and the potential electron transport rate (J), respectively. The reference values were obtained from the parameters from the optimal treatment from A, AN, and N. Here, we adopted the N treatment as the optimal treatment.

Anatomical analysis

After the photosynthetic parameter measurements, leaf pieces (approximately 5mm×5 mm) were cut between the main veins from each of the four different plants for anatomical measurements and transmission electron microscope (TEM) analysis. For anatomical measurement, leaf segments were quickly fixed with FAA (95% ethanol: glacial acetic acid: formalin: distilled water =10:1:2:7, v/v) and dehydrated in dimethylbenzene-ethanol series. The pieces were then staining with safranin-fast green and embedded in paraffin. After cutting into 6 μm transverse sections, the pieces were photographed at a magnification of 400× with Nikon Eclipse E100 microscope equipped with a Nikon microscope camera (Nikon DS-U3). For TEM analysis, leaf materials were quickly fixed with glutaraldehyde (2.5%, v/v) in 0.1 M phosphate buffer (pH 7.4) under vacuum. Afterward, the segments were postfixed

with 2% osmium tetroxide and dehydrated in a graded ethanol series, followed by washing in propylene oxide. The dehydrated segments were then embedded in Epon 812 resin. Ultrathin cross-sections were cut with a Power Tome-XL ultramicrotome, stained with 2% uranyl acetate, and then viewed under an H7650 transmission electron microscope (H-7650, Hitachi, Japan). Photos were taken at 2000-8000× direct magnification to measure the cell wall thickness and chloroplast characteristics. Leaf thickness (T_L), leaf density (D_L), leaf volume per area ($V_A=A_L\times T_L$), mesophyll thickness between two epidermises (T_{mes}), and the volume fraction of intercellular air space (f_{ias}) were calculated according to the light and TEM micrographs. The D_L and f_{ias} were determined as follows:

$$D_L = \frac{M_A}{T_L} \qquad (10)$$

$$f_{ias} = 1 - \frac{\Sigma S_S}{T_{mes}\, W} \qquad (11)$$

where M_A is the specific leaf weight (mg cm^{-2}), ΣS_s is the total cross-section area of the mesophyll cells and W is the width of the measured framed range.

Chloroplast (S_c/S) and mesophyll (S_{mes}/S) surface area exposed to intercellular airspace per unit leaf area were also calculated from light and TEM micrographs, as reported by Evans *et al*. (1994) and Syvertsen *et al*. (1995).

$$S_{mes}/S = \frac{L_{mes}}{W} * F \qquad (12)$$

$$S_c/S = \frac{L_c}{W} * F = \frac{L_c}{L_{mes}} * S_{mes}/S \qquad (13)$$

where the L_{mes} is the total mesophyll surface length facing intercellular air space per leaf area, and L_c is the chloroplast surface length facing intercellular air space per leaf area. F is the curvature correction factor, which depends on the shape of mesophyll cell and was calculated according to Thain (1983). Briefly, according to the differences of palisade and spongy cells (i.e., cell arrangement direction and axial/length ratio), F was calculated as a weight average of spongy (F_1) and palisade (F_2) mesophyll distributions:

$$F_1 = \frac{1+2\,\bar{b}_1/\bar{a}_1}{1+4\,\bar{b}_1/\pi\bar{a}_1} \quad (14)$$

$$F_2 = [(\bar{a}/\bar{b}) + (1/e)\sin^{-1}e]/E \quad (15)$$

where $\bar{a}$ and $\bar{b}$ are the average of the length and thickness of the mesophyll. e is the eccentricity, and E is the elliptical integral, which were calculated as follows, respectively:

$$e = \sqrt{1-(\bar{a})^2/(\bar{b})^2} \quad (16)$$

$$E \approx \frac{\pi}{2}\left(1-\frac{e^2}{4}-\frac{3e^4}{64}-\frac{5e^3}{256}\right) \quad (17)$$

Besides, cell wall thickness (T_{cw}), chloroplast length (L_{chl}) and thickness (T_{chl}), the distance between two neighboring chloroplasts ($D_{chl\text{-}chl}$), chloroplast distance from the cell wall (L_{cyt}), and the chloroplast number per mesophyll cell were measured from TEM micrographs at a 2000-8000×. The images were analyzed with Image-Pro Plus software (Media Cybernetics, Sliver Spring, MD, USA).

g_m modelled from anatomical characteristics

To determine g_m, the one-dimension gas diffusion model modified by Tomas *et al*. (2013) was applied in this study. g_m, a composite conductance, is shared by different leaf anatomical characteristics and decided by within-leaf gas and liquid components:

$$g_m = \frac{1}{\frac{1}{g_{ias}} + \frac{RT_k}{H^* g_{liq}}} \quad (18)$$

where g_{ias} is the gas-phase conductance which stands for the gas-phase pathway from substomatal cavities to the outer surface of cell wall, and g_{liq} is the liquid conductance that from the outer surface of cell wall to chloroplast. R is the gas constant (Pa m^3 K^{-1} mol^{-1}), T_k is the absolute temperature (K), and H is the Henry's law constant (Pa m^3 mol^{-1}). Due to the g_m in this equation, is defined as a gas-phase conductance, thus H/RT_k (dimensionless form of Henry's constant) is needed to convert to g_{liq} to the corresponding gas-phase equivalent conductance (Niinemets and Reichstein, 2003).

In this model, gas-phase conductance depends on gas-phase porosity (f_{ias}) and

effective diffusion path in the gas-phase (ΔL_{ias}):

$$g_{ias} = \frac{1}{r_{ias}} = \frac{D_a * f_{ias}}{\Delta L_{ias} * \varsigma} \qquad (19)$$

where ς is the diffusion path tortuosity (m m^{-1}) and Da (m^2 s^{-1}) is the diffusion coefficient for CO_2 in the gas-phase (1.51×10^{-5} at 25°C). ΔL_{ias} is taken as half of the mesophyll thickness (T_{mes}).

The total liquid-phase diffusion conductance was determined by different components in mesophyll cell, including the conductance in the cell wall (g_{cw}), plasma membrane (g_{st}), cytosol (g_{cyt}), chloroplast envelope (g_{en}), and stroma (g_{st}). Thus, the g_{liq} was given as:

$$g_{liq} = \frac{S_c}{(r_{cw}+r_{pl}+r_{cyt}+r_{en}+r_{st})S} \qquad (20)$$

where r_{cw}, r_{pl}, r_{cyt}, r_{en}, r_{st} are the reciprocal term of g_{cw}, g_{st}, g_{cyt}, g_{en}, g_{st}, respectively. Alternatively, according to Tholen *et al.*(2012b), the CO_2 diffusion inside the cell in different ways: one for cell wall parts with chloroplast ($g_{cel,1}$), and the other for inter-chloroplast areas ($g_{cel,2}$), and the corresponding resistance was expressed as $r_{cel,1}$ and $r_{cel,2}$. Thus, the equation of g_{liq} was converted as:

$$g_{liq} = \frac{S_{mes}}{(r_{cw}+r_{pl}+r_{cel,1}+r_{cel,\ 2})S} \qquad (21)$$

In addition, the conductance of liquid-phase diffusion pathway, either for cell wall (g_{cw}), cytosol (g_{cyt}), or stroma conductance (g_{st}) is given as follows:

$$g_i = \frac{1}{r_i} = \frac{r_{f,i} * D_w * p_i}{\Delta L_i} \qquad (22)$$

where $r_{f,i}$ (dimensionless factor) accounts for the decrease of CO_2 diffusion in the aqueous phase compared with free diffusion in water and was taken as 1.0 for cell wall and 0.3 for cytosol and stroma, as reported by Rondeau-Mouro *et al.*(2018) and Niinemets *et al.*(2003).ΔL_i (m) is the diffusion path length in the corresponding component of the diffusion pathway, and p_i (m^3 m^{-3}) is the effective porosity in the given part. The value of p_i was set to 1.0 for cytosol and stroma, and 0.29 for the cell wall. D_w is the CO_2 diffusion coefficient in aqueous phase (1.79×10^{-9} m^{-2} s^{-1} at 25°C). Besides, conductance of plasma membrane (g_{pl}) and chloroplast envelope (g_{env}) was

assumed as constant value of 0.0035 m s^{-1}(Evans *et al.*, 1994; Tosens *et al.*, 2012b).

The quantitation of the anatomical limitation of the g_m

The determinants of g_m were shared by gas-phase conductance (l_{ias}) and liquid-phase conductance(l_i). The proportion limited by l_{ias} was calculated as:

$$l_{ias} = \frac{g_m}{g_{ias}} \qquad (23)$$

The share of g_m by the cellular-phase conductance (l_i), which stands for the limitation of cell wall, the plasmalemma, and inside the cells was determined as:

$$l_i = \frac{g_m}{g_i * \frac{S_{mes}}{S}} \qquad (24)$$

where g_i is the component diffusion conductance of the corresponding pathways. The fraction of exposed cell wall area lined with chloroplasts and fraction free of chloroplast were used to weighted limitations imposed by different cellular components (cytoplasm, chloroplast envelope, and stroma).

Statistical analysis

Statistical analysis was conducted with SPSS 25.0 (SPSS Inc., Chicago, IL, USA). All data were subjected to a one-way analysis of variance (ANOVA), and the significant differences between treatments were compared using the least significant difference (*LSD*) at $P < 0.05$. Linear regression analyses were used to obtain the relationships among photosynthetic capacity and the main limiting factors, the key structural parameters and mesophyll conductance, and the values of mesophyll conductance estimated from different methods. Graphics and regression analyses were performed using Origin Pro 2021 software (Origin Lab Corporation, Northampton, MA, USA).

Results

Leaf morphology characteristics

Sole NH_4^+ supply significantly decreased leaf area (A_L) and increased leaf thickness (T_L) in comparison with sole NO_3^- and mixed N supply (Table 1). Correspondingly, the leaf volume per area (V_A) of sole NH_4^+ supply was almost half

of the V_A of mixed N supply. The variation in leaf density (D_L) was 1.5-fold with sole NH_4^+ supply having the densest leaves (0.36 g cm^{-3}) and sole NO_3^- supply the least dense (0.27 g cm^{-3}). Notably, M_A seemed uninfluenced among the treatments. The leaf N concentration (N_L) of sole NO_3^- supply was approximately 11% lower compared with mixed N and sole NH_4^+ supply, yet the photosynthetic N use efficiency was dramatically upregulated by NO_3^- treatments.

Leaf physiological characteristics

In comparison to sole NH_4^+ supply, net photosynthetic rate (A) was increased by both sole NO_3^- and mixed N supply, by 39.2% and 26.6%, respectively. Whilst the intercellular CO_2 concentration (C_i) seemed indifferent among the treatments, chloroplast CO_2 concentration (C_c) was significantly down-regulated by sole NH_4^+ supply. For the stomatal conductance (g_s) and mesophyll conductance (g_m), sole NO_3^- and mixed N supply had higher value than sole NH_4^+ supply and coincided with elevated electron transfer rate (J) and carboxylation efficiency (CE) (Table 2).

In order to ascertain the photosynthetic component that had the largest effect on net assimilation rate, we performed a correlation analysis, and the net photosynthesis rate (A) was positively correlated with stomatal conductance (g_s), mesophyll conductance (g_m), and electron transport rate (J) (Figure 2). The CO_2 drawdown (C_i-C_c) from sub-stomatal cavities (C_i) to chloroplasts (C_c) ranged from 86.3 to 107.3 μmol mol^{-1} and was higher in leaves with decreased g_m under sole NH_4^+ supply.

Leaf anatomical traits

Among the leaf ultrastructural characteristics estimated from TEM (Table 3; Figure 1), the mesophyll thickness (T_{mes}), the volume fraction of intercellular air space (f_{ias}), mesophyll surface area (S_{mes}/S), and the chloroplast surface area (S_c/S) exposed to intercellular airspace per unit leaf area were significantly down-regulated by sole NH_4^+ supply. Notably, there were marked differences in cell wall thickness (T_{cw}) among the treatments, for sole NO_3^- supply exhibited the thinnest cell wall (0.16 μm), while sole NH_4^+ supply had the thickness cell walls with the maximum value of

0.25 μm. For chloroplast characteristics, the length (L_{chl}) and thickness (T_{chl}) of the chloroplasts, and the distance of the chloroplast from the cell wall (L_{cyt}) seemed unaffected by N forms supply, whereas NH_4^+ supply significantly elevated the distance between adjacent chloroplasts ($D_{chl\text{-}chl}$). Besides, chloroplasts amount in per sponge cell and palisade cell showed more specific changes among the treatments. In the comparison with the other treatments, chloroplasts of both sponge and palisade cell were dramatically up-regulated in sole NO_3^- supply (Supplementary Figure S1).

Besides, g_m was not correlated with T_{mes}, reflecting the circumstance that T_{mes} seemed more invariable. The positive and significant correlation between g_m and S_c/S, f_{ias} were observed, combined with the negative relationship observed between g_m and T_{cw} suggested the importance of anatomical components to the intercellular CO_2 diffusion.

Estimation of g_m with different methods

In the present study, the value of g_m was measured according to the gas exchange and chlorophyll fluorescence (Harley *et al*., 1992), and compared with g_m modelled by A/C_i response curves (Bernacchi *et al.*, 2002) and anatomical characteristics (Tomás *et al.*, 2013). The correlation analysis indicated that the estimated g_m from different methods was mainly positively correlated (Supplementary Figure S3). However, the slope was different from unity, and the Harley *et al*.-based and Tomás *et al*.-based estimates of g_m were strongly correlated with a R^2 of 0.76 ($P < 0.01$).

Limiting components analyses of *A*

The relative limitations of stomatal conductance(l_s), mesophyll diffusion (l_m), and biochemistry capacity (l_b) on photosynthesis are shown in Figure 3(a). In the NO_3^-treatment and mixed N treatment, the percentages of the three limiting components are relatively close, and l_b (36.4% and 39.5%, respectively) accounts for the most important relative limitation of photosynthesis. While for sole NH_4^+ supply, the relative limitation of l_s, l_m, and l_b significantly varied, and the l_m (44.2%) was considered more important of photosynthesis, followed by l_s (30.8%) and l_b (25.0%).

Meanwhile, according to quantitative limitations analysis of *A*, mesophyll conductance limitation (MC_L) was the highest constrain of *A* under sole NH_4^+ supply, accounting for the 24.39 % of *A* decline compared with the NO_3^- treatment (Figure 3).

Key structural factors regulating *A* through g_m

For the different components of the whole CO_2 diffusion pathway, restrictions in liquid-phase CO_2 conductance were the dominant limiting factors on g_m, accounting for approximately 90% of the total limitation (Figure 4b). Among the different components of the liquid-phase, the stroma limitation was the main limiting factor in the liquid-phase, whereas the stroma limitation seemed unaffected by the treatments. The liquid-phase limiting component of g_m is also associated with the cytoplasm, with significantly upregulated by sole NH_4^+ supply. In comparison with the sole NH_4^+ supply, plasma membrane and chloroplast envelope limitation proposed a slightly higher percentage in sole NO_3^- supply, with 24.3% and 24.3%, respectively. For the absolute value of the limitations, the cell walls appeared to have a more specific change among the treatments that limited the internal diffusion of CO_2 varied from 303.69 to 480.37 s m^{-1} (Figure 4a). Besides, the variation in cytoplasm resistance was 1.7-fold, with sole NO_3^- treatment having the lowest resistance (450.13 s m^{-1}) and sole NH_4^+ supply having the highest (664.23 s m^{-1}).

Discussion

g_m dominated the decrease of *A* in sole NH_4^+ supply

In the present study, inorganic N sources significantly decreased the photosynthetic rate (*A*) of *Lonicera Japonica*. Leaf in sole NH_4^+ treatment was observed a dramatically downregulated *A*, in parallel with a larger dropdown of CO_2 from the sub-stomatal cavities (C_i) to the sites of carboxylation inside the chloroplasts (C_c). Among the limiting factors, mesophyll conductance limitation (MC_L) controlled 60.3 % of *A* decline, followed by stomatal conductance (S_L, 26.4%) and biochemistry limitation (B_L, 13.3%). These results suggested the mesophyll diffusion resistance to CO_2 is a key limiting factor to *A*. Early studies suggested that g_m was driven by

integrated leaf characteristics, notably and negatively correlated with leaf mass per area (M_A) (Flexas *et al.*, 2008; Han, 2011; Niinemets *et al.*, 2009a; Onoda *et al.*, 2017). Nevertheless, the M_A did not show any significant difference among treatments in this study, despite some declining tendency of sole NO_3^- treatment. Whist the unchanged M_A, the present data showed that the NH_4^+-fed leaves were manifested by higher leaf thickness (T_L)and density (D_L), and a smaller leaf area (A_L) and leaf volume (V_A) (Table 1). The leaf traits are generally observed in NH_4^+-fed plants compared to those supplied with NO_3^- (Guo *et al.*, 2007), suggesting the high leaf structure plasticity and varied leaf carbon-expensive structure in relation to environmental conditions.

As there is ample agreement that the use of integrated traits such as M_A as proxies of g_m might not be valid in all cases, the intercellular anatomical traits that limit CO_2 effective diffusion length and area, in particularly the cell wall thickness (T_{cw}) are especially crucial (Evans *et al.*, 2009; Momayyezi and Guy, 2017; Tosens *et al.*, 2012b). In the present study, a one-dimensional within-leaf gas diffusion model considering all of the leaf anatomical limitations was applied as previously modified by Tomas *et al*. (2013). The g_m modelled from anatomical traits was tightly correlated with measured g_m (Supplementary Figure S3), which, to some extent, verified the view that the variation of g_m is related to the intercellular structures involved in CO_2 diffusion. Nevertheless, the partial conductance components are generally assumed to be composed of a single medium in the estimation of g_m, which might be unrealistic (Gago *et al.*, 2020). In addition, the carbonic anhydrases, as well as aquaporins were not considered in the g_m-modelled (Flexas *et al.*, 2012). Consequently, the correlation between g_m-gas exchanges and g_m-modelled frequently deviates from the 1:1 relationship.

Mesophyll conductance is a composite conductance of an intercellular gas-phase (g_{ias}) and a liquid-phase (g_{liq}). The g_{ias} mainly depends on the intercellular air space and mesophyll thickness, while the g_{liq} was affected by apoplast and cellular components of the CO_2 pathway, which can be scaled by the chloroplast surface area

exposed to intercellular air space per unite leaf area (S_c/S) (Flexas *et al.*, 2012). It was observed that the limitations were mainly represented by liquid-phase, and the gas-phase accounts for only approximately 10% (Figure 4b), analogous to the value obtained in rape (Lu *et al.*, 2016). Despite the low proportion, a significant discrepancy of g_{ias} among the treatments appeared, in that gas-phase limitation was upregulated by sole NH_4^+ supply. This result was somewhat inconsistent with Liu *et al* (2021) and Gao *et al* (2020), as NO_3^- caused higher limitation on g_{ias}. This could be explained by the variation of the environment light intensity, concentrations of N addition, experiment period as well as the plant species. Integrated all the determinants into account, there was a positive correlation between g_m and the volume fraction of intercellular air space (f_{ias}) ($R^2 = 0.71$, $P < 0.01$), while a weak relationship with the mesophyll thickness (Figure 5), suggesting that f_{ias} was more variable in regulating g_m. Additionally, f_{ias} under sole NO_3^- supply was approximately 2-folds higher than that of sole NH_4^+ supply, similar to the result of Liu *et al* (2021). The flexible f_{ias} were general in plants, which may be ascribed to acclimation-related changes, e.g., a larger f_{ias} was usually observed in more favorable growth conditions (Binks *et al.*, 2016; Muller *et al.*, 2009).

Structural trade-off in driving the share of *A* limitations

As suggested in various studies, S_c/S is more influential in determining g_m across species (Loucos *et al.*, 2017; Ren *et al.*, 2019; Terashima *et al.*, 2011; Veromann-Jürgenson *et al.*, 2020; Veromann-Jurgenson *et al.*, 2017). Here, the down-regulation of S_c/S by sole NH_4^+ supply was speculated to be attributed to the fewer chloroplast numbers and the lower mesophyll surface area exposed to intercellular airspace per leaf area (S_{mes}/S) (Table 3), similar to the observation of (Carriqui *et al.*, 2015); while the length and thickness of chloroplasts were unchanged among the treatments. Despite the dropdown of r_{st}, a fact that cannot be ignored is the relative control of chloroplast stroma on g_{liq} was less affected by N forms, with no significant change among the treatments.

There rises a crucial concern that whether g_m was necessarily controlled by the component owning the largest proportion, because the contribution of components that limit CO_2 diffusion may vary among species. Here, the discrepancy in liquid-phase resistance was suggested to be related to the cytoplasm and cell wall. For cytoplasm, it accounts for approximately 15% of liquid resistance in the present study, corresponds well with previous reports (Lu *et al.*, 2016; Tosens *et al.*, 2012a; Tosens *et al.*, 2012b). Commonly, the chloroplasts are arranged against the cell periphery to absorb light and CO_2 (Sage *et al.*, 2009), thus the distance of chloroplast from cell wall (L_{cyt}) could be responsible for most of the cytoplasm resistance, as reported by (Sharkey *et al.*, 1991). However, L_{cyt} was the same among the treatments (Table 3) in this study, and therefore, the upregulated r_{cyt} in NH_4^+ treatment may be explained by the increase of distance between adjacent chloroplasts ($D_{chl\text{-}chl}$), by up to 50% compared with mixed N treatment.

Previous studies have highlighted the importance of cell wall in determining g_m among species, as the cell wall could account for 50% of g_m by restricting CO_2 diffusion (Evans *et al.*, 2009; Terashima *et al.*, 2006). Although the limitation is often neglected, cell wall limitation sometimes is greater than S_c/S, and together these constitute the primary anatomical factors for setting the maximum g_m (Carriquí *et al.*, 2019; Carriqui *et al.*, 2019). Here, the cell wall thickness (T_{cw}) varied over a range of 0.16 to 0.25 μm, and T_{cw} of sole NO_3^- treatment decreased by 27% to 36% in the comparison with mixed N and sole NH_4^+ supply, resulting in a dramatic difference among the treatments. Głazowska *et al*. (2019) had reported that the distinct cell wall remodeling was mediated by inorganic N supply. NH_4^+-mediated cell wall thicken, as observed in early studies may be ascribed to changes in the contents of polysaccharide, ion, lignin, or cellulose of cell walls (Ellsworth *et al.*, 2018; Podgórska *et al.*, 2017). Meanwhile, as previously mentioned, a more rigid cell wall structure could explain the reduction in A_L in ammonium supply, by limiting cell expansion. Besides, the T_{cw} and g_m were observed strongly and positively correlation in this study (Figure 5 (b),

R^2 = 0.53, P < 0.01), the reduced g_m and thicker cell wall were reported to be an adaption of plant species to dry or nutrition poor environment (Niinemets *et al.*, 2009a; Niinemets *et al.*, 2009b).

Recent evidence points to an effect of cell wall composition on photosynthesis, possibly due to a trade-off of N allocation between chloroplasts and the cell wall in plants (Kuusk *et al.*, 2018). In angiosperms, particular in C3 plants, chloroplast N distribution accounts for almost 75 %, while the cell wall for 10% (Li *et al.*, 2017; Onoda *et al.*, 2017; Wang *et al.*, 2015); the leaf N that is not allocated to photosynthetic apparatus is generally used structurally in cell walls (Feng *et al.*, 2009). In this study, the reduced chloroplasts numbers and the thicker T_{cw} by sole NH_4^+ supply were speculated to be related to the down-regulated photosynthetic N allocation (Figure S1). Takashima *et al* (2004) had reported that higher N allocation to the cell wall could lead to decreased PNUE. The discrepancy of N partitioning among N sources may indicate a trade-off in the leaf photosynthetic capacity and the persistence, while the mechanism underlying this result need further research.

Conclusion

The present study showed that N sources significantly affected the leaf morphology and photosynthetic rate (A) of *L. Japonica* and suggested the mesophyll diffusion resistance accounts for the most limiting of A, with more than 50%. Sole NH_4^+-fed leaves were characterized by smaller leaf area, higher leaf thickness, and larger leaf density. Variations of mesophyll conductance (g_m) under different N sources were ascribed to the leaf anatomy changes, notably the internal air space (f_{ias}), exposed surface area of chloroplasts per unit leaf area (S_c/S) and cell wall thickness (T_{cw}). Ammonium treatment reduced the f_{ias} and chloroplast numbers, resulting in an increased intercellular length and inter-chloroplast length, and finally inhibition of g_m and A (Figure 6).

Acknowledgments

This work was financially supported by the National Natural Science Foundation of China (32072673), the Fundamental Research Funds for the Central Universities (KYGD202007), the Young Elite Scientists Sponsorship Program by CAST (2018QNRC001), and the Innovative Research Team Development Plan of the Ministry of Education of China (IRT_17R56).

Author contributions

Shiwei Guo and Yiwen Cao conceived the idea and designed the experiment; Yiwen Cao, Yonghui Pan, and Tianheng Liu completed the experiment; Yiwen Cao analyzed the data and wrote the manuscript; Shiwei Guo, Min Wang, and Yonghui Pan helped in manuscript revising; Shiwei Guo and Min Wang provided funding support. All the authors contributed critically to the drafts and gave final approval for publication.

Conflict of interest

The authors declare that the research was conducted in the absence of any commercial or financial relationships that could be construed as a potential conflict of interest.

Reference

Baginsky, S. and Gruissem, W.J. 2004. Chloroplast proteomics: potentials and challenges. *Journal of Experimental Botany* **55,** 1213-1220.

Bino, R.J., De Vos, C.R., Lieberman, M., Hall, R.D., Bovy, A., Jonker, H.H., Tikunov, Y., Lommen, A., Moco, S. and Levin, I.J. 2005. The light-hyperresponsive high pigment-2dg mutation of tomato: alterations in the fruit metabolome. *New Phytologist* **166,** 427-438.

Carpita, N., Sabularse, D., Montezinos, D. and Delmer, D.P.J.S. 1979. Determination of the pore size of cell walls of living plant cells. *Science* **205,** 1144-1147.

Carriquí, M., Nadal, M., Clemente-Moreno, M.J., Gago, J., Miedes, E. and Flexas, J. 2020. Cell wall composition strongly influences mesophyll conductance in gymnosperms. *The plant journal* **103,** 1372-1385.

Carriqui, M., Cabrera, H.M., Conesa, M.A., *et al.* 2015. Diffusional limitations explain the lower photosynthetic capacity of ferns as compared with angiosperms in a common garden study. *Plant Cell & Environment* **38,** 448-460.

Carriquí, M., Douthe, C., Molins, A. and Flexas, J. 2019. Leaf anatomy does not explain apparent short-term responses of mesophyll conductance to light and CO_2 in tobacco. *Physiologia Plantarum* **165,** 604-618.

Carriqui, M., Roig-Oliver, M., Brodribb, T.J., *et al*. 2019. Anatomical constraints to nonstomatal diffusion conductance and photosynthesis in lycophytes and bryophytes. *New Phytologist* **222,** 1256-1270.

Carpita, N., Sabularse, D., Montezinos, D. and Delmer, D.P. 1979. Determination of the pore size of cell walls of living plant cells. *Science* **205,** 1144-1147.

Ellsworth, P.V., Ellsworth, P.Z., Koteyeva, N.K. and Cousins, A.B. 2018. Cell wall properties in *Oryza* sativa influence mesophyll CO_2 conductance. *New Phytologist* **219,** 66-76.

Evans, J.R. and Clarke, V.C. 2019. The nitrogen cost of photosynthesis. *Journal of Experimental Botany* **70,** 7-15.

Evans, J.R., Kaldenhoff, R., Genty, B. and Terashima, I.J. 2009. Resistances along the CO_2 diffusion pathway inside leaves. *Journal of Experimental Botany* **60,** 2235-2248.

Evans, J.R., Voncaemmerer, S., Setchell, B.A. and Hudson, G.S. 1994. The relationship between CO_2 trnsfer conductance and leaf anatomy intransgenics tobacco with a resuced content of Rubisco. *Australian Journal of Plant Physiology* **21,** 475-495.

Feng, Y.L., Lei, Y.B., Wang, R.F., Callaway, R.M., Valiente-Banuet, A., Inderjit, Li, Y.P. and Zheng, Y.L. 2009. Evolutionary tradeoffs for nitrogen allocation to photosynthesis versus cell walls in an invasive plant. *Proceedings of the National Academy of Sciences of the United States of America* **106,** 1853-1856.

Flexas, J., Barbour, M.M., Brendel, O., Cabrera, H.M., Carriquí, M., Díaz-Espejo, A., Douthe, C., Dreyer, E., Ferrio, J.P. and Gago, J.J. 2012. Mesophyll diffusion conductance to CO_2: an unappreciated central player in photosynthesis. *Plant Science* **193,** 70-84.

Flexas, J., Clemente-Moreno, M.J., Bota, J., Brodribb, T.J., Gago, J., Mizokami, Y., Nadal, M., Perera-Castro, A.V., Roig-Oliver, M. and Sugiura, D.J. 2021. Cell wall thickness and composition are involved in photosynthetic limitation. *Journal of Experimental Botany* **72,** 3971-3986.

Flexas, J., Ribas-Carbo, M., Diaz-Espejo, A., Galmes, J. and Medrano, H. 2008. Mesophyll conductance to CO_2: current knowledge and future prospects. *Plant Cell & Environment* **31,** 602-621.

Gago, J., Daloso, D., Carriquí, M., Nadal, M., Morales, M., Araújo, W., Nunes-Nesi, A., Perera-Castro, A., Clemente-Moreno, M., Flexas, J.J. 2020. The photosynthesis game is in the" inter-play": mechanisms underlying CO_2 diffusion in leaves. *Environmental and Experimental Botany*, **178,** 104174.

Gao, L., Lu, Z., Ding, L., Xie, K., Wang, M., Ling, N. and Guo, S. 2020. Anatomically induced changes in rice leaf mesophyll conductance explain the variation in photosynthetic nitrogen use efficiency under contrasting nitrogen supply. *BMC Plant Biology* **20,** 527.

Głazowska, S., Baldwin, L., Mravec, J., Bukh, C., Fangel, J.U., Willats, W.G. and Schjoerring, J.K. 2019. The source of inorganic nitrogen has distinct effects on cell wall composition in Brachypodium distachyon. *Journal of experimental botany* **70,** 6461-6473.

Golvano, M., Felipe, M. and Cintas, A.J. 1982. Influence of nitrogen sources on chloroplast development in wheat seedlings. *Physiologia Plantarum* **56,** 353-360.

Guo, S., Zhou, Y., Shen, Q., and Zhang, F. 2007. Effect of ammonium and nitrate nutrition on some physiological processes in higher plants-growth, photosynthesis, photorespiration, and water relations. *Plant Biology*, 9(01), 21-29.

Hikosaka, K.J. 2004. Interspecific difference in the photosynthesis–nitrogen relationship: patterns, physiological causes, and ecological importance. *Journal of plant research* **117,** 481-494.

Hu, W., Lu, Z., Meng, F., Li, X., Cong, R., Ren, T., Sharkey, T.D. and Lu, J. 2020. The reduction in leaf area precedes that in photosynthesis under potassium deficiency: the importance of leaf anatomy. *New Phytologist* **227,** 1749-1763.

Kuusk, V., Niinemets, Ü. and Valladares, F.J. 2018. Structural controls on photosynthetic capacity through juvenile-to-adult transition and needle ageing in Mediterranean pines. *The Plant Cell* **32,** 1479-1491.

Li, L., Nelson, C.J., Trösch, J., Castleden, I., Huang, S. and Millar, A.H. 2017. Protein degradation rate in Arabidopsis thaliana leaf growth and development. **29,** 207-228.

Liu, M., Liu, X., Du, X., Korpelainen, H., Niinemets, U. and Li, C. 2021. Anatomical variation of mesophyll conductance due to salt stress in Populus cathayana females and males growing under different inorganic nitrogen sources. *Tree*

618 *physiology* **41,** 1462-1478.

619 **Long, S.P. and Bernacchi, C.J.** 2003. Gas exchange measurements, what can
620 they tell us about the underlying limitations to photosynthesis? Procedures and
621 sources of error. *Journal of Experimental Botany* **54,** 2393-2401.

622 **Loucos, K.E., Simonin, K.A., Barbour, M.M.** 2017. Leaf hydraulic
623 conductance and mesophyll conductance are not closely related within a single
624 species. *Plant Cell & Environment* **40,** 203-215.

625 **Lu, Z., Lu, J., Pan, Y., Lu, P., Li, X., Cong, R. and Ren, T.** 2016. Anatomical
626 variation of mesophyll conductance under potassium deficiency has a vital role in
627 determining leaf photosynthesis. *Plant Cell & Environment* **39,** 2428-2439.

628 **M. Weraduwage, S., Kim, S.-J., Renna, L., C. Anozie, F., D. Sharkey, T. and**
629 **Brandizzi, F.J.** 2016. Pectin methylesterification impacts the relationship between
630 photosynthesis and plant growth. *Plant Physiology* **171,** 833-848.

631 **Momayyezi, M. and Guy, R.D.** 2017. Substantial role for carbonic anhydrase in
632 latitudinal variation in mesophyll conductance of Populus trichocarpa Torr. & Gray.
633 *Plant Cell & Environment* **40,** 138-149.

634 **Niinemets, Ü., Diaz-Espejo, A., Flexas, J., Galmes, J. and Warren, C.R.**
635 2009a. Role of mesophyll diffusion conductance in constraining potential
636 photosynthetic productivity in the field. *Journal of Experimental Botany* **60,**
637 2249-2270.

638 **Niinemets, Ü., Wright, I.J. and Evans, J.R.** 2009b. Leaf mesophyll diffusion
639 conductance in 35 Australian sclerophylls covering a broad range of foliage structural
640 and physiological variation. *Journal of experimental botany* **60,** 2433-2449.

641 **Niinemets, Ü. and Reichstein, M.** 2003. Controls on the emission of plant
642 volatiles through stomata: A sensitivity analysis. *Journal of Geophysical*
643 *Research-Atmospheres* **108**.

644 **Niinemets, Ü.** 2001. Global-scale climatic controls of leaf dry mass per area,
645 density, and thickness in trees and shrubs. *Ecology* **82,** 453-469.

Onoda, Y., Wright, I.J., Evans, J.R., Hikosaka, K., Kitajima, K., Niinemets, U., Poorter, H., Tosens, T. and Westoby, M. 2017. Physiological and structural tradeoffs underlying the leaf economics spectrum. *New Phytologist* **214,** 1447-1463.

Peguero-Pina, J.J., Siso, S., Flexas, J., Galmes, J., Garcia-Nogales, A., Niinemets, U., Sancho-Knapik, D., Saz, M.A. and Gil-Pelegrin, E. 2017. Cell-level anatomical characteristics explain high mesophyll conductance and photosynthetic capacity in sclerophyllous Mediterranean oaks. *New Phytologist* **214,** 585-596.

Pegueri-Pina, J.J., Flexas, J., Galmes, J., Niinemets, U., Sancho-Knapik, D., Barredo, G., Villarroya, D. 2012. Leaf anatomical properties in relation to differences in mesophyll conductance to CO_2 and photosynthesis in two related Mediterranean Abies species. *Plant, Cell & Environment* **35,** 2121-2129.

Perchlik, M. and Tegeder, M.J. 2018. Leaf amino acid supply affects photosynthetic and plant nitrogen use efficiency under nitrogen stress. *Plant Physiology* **178,** 174-188.

Podgórska, A., Burian, M., Gieczewska, K., Ostaszewska-Bugajska, M., Zebrowski, J., Solecka, D. and Szal, B.J. 2017. Altered cell wall plasticity can restrict plant growth under ammonium nutrition. *Frontiers in plant science* **8,** 1344.

Pons, T.L., Flexas, J., Von Caemmerer, V. S., Evans, J.R., Genty, B., Ribas-Carbo, M. and Brugnoli, E.J. 2009. Estimating mesophyll conductance to CO_2: methodology, potential errors, and recommendations. *Journal of Experimental Botany* **60,** 2217-2234.

Poorter, H., Niinemets, Ü., Poorter, L., Wright, I.J. and Villar, R.J. 2009. Causes and consequences of variation in leaf mass per area (LMA): a meta-analysis. *New phytologist* **182,** 565-588.

Ren, T., Weraduwage, S.M. and Sharkey, T.D. 2019. Prospects for enhancing leaf photosynthetic capacity by manipulating mesophyll cell morphology. *Journal of Experimental Botany* **70,** 1153-1165.

Rondeau-Mouro, C., Defer, D., Leboeuf, E. and Lahaye, M. 2008.

674 Assessment of cell wall porosity in Arabidopsis thaliana by NMR spectroscopy.
675 *International Journal of Biological Macromolecules* **42,** 83-92.

676 **Sage, T.L. and Sage, R.F.** 2009. The functional anatomy of rice leaves:
677 implications for refixation of photorespiratory CO_2 and efforts to engineer C4
678 photosynthesis into rice. *Plant and Cell Physiology* **50,** 756-772.

679 **Sartory, D.P. and Grobbelaar, J.U.** 1984. Extraction of chlorophyll a from
680 freshwater phytoplankton for spectrophotometric analysis. *Hydrobiologia* **114,**
681 177-187.

682 **Schierenbeck, K.A.** 2004. Japanese honeysuckle (*Lonicera japonica*) as an
683 invasive species; History, ecology, and context. *Critical Reviews in Plant Sciences* **23,**
684 391-400.

685 **Shang, X.F., Pan, H., Li, M.X., Miao, X.L. and Ding, H.** 2011. *Lonicera*
686 *japonica* Thunb.: Ethnopharmacology, phytochemistry and pharmacology of an
687 important traditional Chinese medicine. *Journal of Ethnopharmacology* **138,** 1-21.

688 **Sharkey, T.D., Vassey, T.L., Vanderveer, P.J. and Vierstra, R.D.** 1991. Carbon
689 metabolism enzymes and photosynthesis in transgenic tobacco (*Nicotiana tabacum* L.)
690 having excess phytochrome. *Planta* **185,** 287-296.

691 **Syvertsen, J.P., Lloyd, J., McConchie, C., Kriedemann, P.E. and Farquhar,**
692 **G.D.** 1995. On the relationship between leaf antomy and CO_2 diffusion through th
693 emesophyll of hypostomatous leaves. *Plant Cell & Environment* **18,** 149-157.

694 **Terashima, I., Hanba, Y.T., Tazoe, Y., Vyas, P. and Yano, S.J.** 2006. Irradiance
695 and phenotype: comparative eco-development of sun and shade leaves in relation to
696 photosynthetic CO_2 diffusion. *Journal of Experimental Botany* **57,** 343-354.

697 **Terashima, I., Hanba, Y.T., Tholen, D. and Niinemets, Ü.** 2011. Leaf
698 Functional Anatomy in Relation to Photosynthesis. *Plant Physiology* **155,** 108-116.

699 **Thain, J.J.** (1983) Curvature correction factors in the measurement of cell
700 surface areas in plant tissues1. *Journal of Experimental Botany* **34,** 87-94.

701 **Tholen, D., Boom, C. and Zhu, X.-G.** 2012a. Opinion: Prospects for improving

photosynthesis by altering leaf anatomy. *Plant Science* **197,** 92-101.

Tholen, D., Ethier, G., Genty, B., Pepin, S. and Zhu, X.G. 2012b. Variable mesophyll conductance revisited: theoretical background and experimental implications. *Plant Cell & Environment* **35,** 2087-2103.

Tomás, M., Flexas, J., Copolovici, L., Galmés, J., Hallik, L., Medrano, H., Ribas-Carbó, M., Tosens, T., Vislap, V. and Niinemets, Ü. 2013. Importance of leaf anatomy in determining mesophyll diffusion conductance to CO_2 across species: quantitative limitations and scaling up by models. *Journal of Experimental Botany* **64,** 2269-2281.

Tosens, T., Niinemets, U., Vislap, V., Eichelmann, H. and Diez, P.C. 2012a. Developmental changes in mesophyll diffusion conductance and photosynthetic capacity under different light and water availabilities in Populus tremula: how structure constrains function. *Plant Cell & Environment* **35,** 839-856.

Tosens, T., Niinemets, U., Westoby, M. and Wright, I.J. 2012b. Anatomical basis of variation in mesophyll resistance in eastern Australian sclerophylls: news of a long and winding path. *Journal of Experimental Botany* **63,** 5105-5119.

Tosens, T., Nishida, K., Gago, J., *et al*. 2016. The photosynthetic capacity in 35 ferns and fern allies: mesophyll CO_2 diffusion as a key trait. *New Phytologist* **209,** 1576-1590.

Veromann-Jürgenson, L.-L., Brodribb, T.J., Niinemets, Ü. and Tosens, T.J. 2020. Variability in the chloroplast area lining the intercellular airspace and cell walls drives mesophyll conductance in gymnosperms. *Journal of Experimental Botany* **71,** 4958-4971.

Veromann-Jurgenson, L.L., Brodribb, T.J., Niinemets, Ü. and Tosens, T. 2020a. Pivotal Role of Mesophyll Conductance in Shaping Photosynthetic Performance across 67 Structurally Diverse Gymnosperm Species. *International Journal of Plant Sciences* **181,** 116-128.

Veromann-Jurgenson, L.L., Brodribb, T.J., Niinemets, Ü. and Tosens, T.

2020b. Variability in the chloroplast area lining the intercellular airspace and cell walls drives mesophyll conductance in gymnosperms. *Journal of Experimental Botany* **71,** 4958-4971.

Veromann-Jurgenson, L.L., Tosens, T., Laanisto, L. and Niinemets, Ü. 2017. Extremely thick cell walls and low mesophyll conductance: welcome to the world of ancient living! *Journal of Experimental Botany* **68,** 1639-1653.

Wang, F., Gao, J.W., Shi, S.M., He, X.H. and Dai, T.B. 2019. Impaired electron transfer accounts for the photosynthesis inhibition in wheat seedlings (*Triticum aestivum* L.) subjected to ammonium stress. *Physiologia Plantarum* **167,** 159-172.

Wang, M., Herrmann, C.J., Simonovic, M., Szklarczyk, D. and von Mering, C. 2015. Version 4.0 of PaxDb: protein abundance data, integrated across model organisms, tissues, and cell-lines. *Proteomics* **15,** 3163-3168.

Xie, K., Lu, Z., Pan, Y., Gao, L., Hu, P., Wang, M. and Guo, S. 2020. Leaf photosynthesis is mediated by the coordination of nitrogen and potassium: the importance of anatomical-determined mesophyll conductance to CO_2 and carboxylation capacity. *Plant Science* **290,** 110267.

Xiong, D., Liu, X., Liu, L., Douthe, C., Li, Y., Peng, S. and Huang, J. 2015. Rapid responses of mesophyll conductance to changes of CO_2 concentration, temperature and irradiance are affected by N supplements in rice. *Plant Cell & Environment* **38,** 2541-2550.

Tables

Table 1. Effect of different N forms on integral leaf variables

Treatment	M_A (mg cm^{-2})	V_A (cm^3)	T_L(μm)	D_L (g cm^{-3})	A_L (cm^2)	Chl (mg g^{-1})	N_a (g m^{-2})	PNUE (μmol g^{-1} s^{-1})
A	4.45±0.49a	0.10±0.02b	114.7±10.5a	0.36±0.06a	8.43±1.48b	4.01±0.76a	1.53±0.12a	9.52±1.97c
AN	4.76±1.46a	0.20±0.02a	106.5±9.6b	0.40±0.12a	13.81±1.83a	4.18±0.42a	1.43±0.21a	13.16±1.70b
N	4.01±0.71a	0.19±0.03a	108.9±9.9b	0.27±0.04b	13.32±0.93a	4.36±0.60a	1.18±0.11b	16.87±1.80a

M_A, leaf mass per area; V_A, leaf volume per area; T_L, leaf thickness; D_L, leaf density; A_L, leaf area; Chl, total chlorophyll concentration per leaf; N_a, leaf nitrogen content per area; PNUE, photosynthetic nitrogen use efficiency, PNUE= A/N_a. A, AN, and N represent the sole NH_4^+ supply, mixed N supply, and sole NO_3^- supply, respectively. Data are mean ± SD of 4 replications. Different letters indicate statistically significant differences ($P < 0.05$).

Table 2. CO_2 transmission characteristics of *L. Japonica* affected by different N forms

Treatment	A (μmol·m^{-2}·s^{-1})	g_s (mol m^{-2} s^{-1})	C_i (μmol mol^{-1})	C_c (μmol mol^{-1})	C_i-C_c (μmol mol^{-1})	g_m (mol m^{-2} s^{-1})	J (μmol m^{-2} s^{-1})	CE
A	14.3±0.9b	0.23±0.05b	277.0±14.6a	160.8±13.6b	107.3±16.2a	0.13±0.03b	122.8±8.4b	0.070±0.005b
AN	18.1±2.5a	0.35±0.10a	275.1±11.8a	188.8±8.0a	86.3±7.9b	0.21±0.04a	138.3±13.4ab	0.085±0.006a
N	19.9±0.5a	0.35±0.01a	266.8±3.1a	177.7±2.0a	89.1±4.2b	0.22±0.01a	156.4±4.4a	0.095±0.011a

A, net photosynthetic rate; g_s, stomatal conductance; C_i, intercellular CO_2 concentration; C_c, chloroplast CO_2 concentration; C_i-C_c, CO_2 drawdown from sub-stomatal cavities (C_i) to chloroplasts (C_c); g_m, mesophyll conductance; *J*, electron transfer rate; *CE*, carboxylation efficiency. A, AN, and N represent the sole NH_4^+ supply, mixed N supply, and sole NO_3^- supply, respectively. Data are mean ± SD of 5 replications for *A*, g_s, C_i, C_c, C_i-C_c, g_m, *J*, and of 4 replications for *CE*; Different letters indicate statistically significant differences ($P < 0.05$).

Table 3. Leaf anatomical structure of *L. Japonica* affected by different N forms

Treatment	T_{mes} (μm)	T_{cw} (μm)	L_{chl} (μm)	T_{chl} (μm)	$D_{chl\text{-}chl}$ (μm)	L_{cyt} (μm)	f_{ias} (%)	S_{mes}/S (m^2 m^{-2})	S_c/S (m^2 m^{-2})
A	83.5±7.5b	0.25±0.02a	6.10±0.96a	2.03±0.20a	1.08±0.04a	0.21±0.03a	17.1±4.3b	11.4±0.4b	6.16±0.21b
AN	83.5±4.1b	0.22±0.03b	5.54±0.47a	1.98±0.22a	0.72±0.03b	0.20±0.03a	33.4±0.03a	13.8±0.4a	8.96±0.20a
N	86.3±4.4a	0.16±0.02c	5.58±0.58a	1.77±0.15a	0.84±0.03b	0.19±0.04a	37.0±2.3a	12.8±0.4a	9.44±0.43a

T_{mes}, mesophyll thickness; T_{cw}, cell wall thickness; L_{chl}, chloroplast length; T_{chl}, chloroplast thickness; $D_{chl–chl}$, the distance between adjacent chloroplasts; L_{cyt}, the distance of chloroplast from cell wall; f_{ias}, the volume fraction of intercellular air space; S_{mes}/S, mesophyll surface area exposed to intercellular airspace per unit leaf area; S_c/S, chloroplast surface area exposed to intercellular air space per leaf area. A, AN, and N represent the sole NH_4^+ supply, mixed N supply, and sole NO_3^- supply, respectively. Data are mean ± SD with 20 microscopic pictures for T_{mes}, f_{ias}, S_{mes}/S, S_c/S, and at least 30 microscopic pictures for the other ultrastructural traits; Different letters indicate statistically significant differences ($P < 0.05$).

Figure legends

Figure 1. Light micrographs (a, e, i, scale bar = 50 μm) and transmission electron micrographs (b, f, j, c, g, k, scale bar = 2 μm; h, scale bar =1 μm; d, l, scale bar = 800 nm) of *L. Japonica* leaves affected by different forms of N, sole NH_4^+ supply (Fig. a-d), mixed N supply (Fig. e-h), and sole NO_3^- supply (Fig. i-l). ias: intercellular air space; SG: starch granule; CW: cell wall; G: grana.

Figure 2. Correlation of the net photosynthetic rate(A) and mesophyll conductance (g_m) **(a),** stomatal conductance (g_s) **(b),** electron transport rate (J) **(c)**, and the relationship between CO_2 drawdown (C_i-C_c) from sub-stomatal cavities (C_i) to chloroplasts (C_c)and g_m **(d)**. A, AN, and N represent the sole NH_4^+ supply, mixed N supply, and sole NO_3^- supply, respectively, corresponding to the symbol of the open triangles, the closed circles, and the open square in the plot. The data were fitted by linear regressions ($P < 0.01$).

Figure 3. Relative limitation of stomatal conductance (l_s), mesophyll diffusion (l_m), and biochemical capacity (l_b) of *L. Japonica* under sole NH_4^+ supply **(a)**, mixed N supply **(b),** and sole NO_3^- supply treatment **(c)**, the limitation of l_s, l_m, and l_b together add up to 100% at each treatment occasions; Quantitative limitation analyses of stomatal limitation (S_L), mesophyll conductance limitation (MC_L), and biochemical limitation (B_L) of *L. Japonica* photosynthesis under sole NH_4^+ supply **(d)**, the data outside the circles represent the absolute quantitative limitations and the data inside the circles represent the share of the total limitations by S_L, MC_L, and B_L.

Figure 4. Anatomical limitations of mesophyll conductance (g_m) **(a)** and the share of the overall g_m limitation **(b)** by cell wall (cw), plasma membrane (pl), chloroplast envelope (env), stroma (st), and cytoplasm (cyt) in leaves of *L. Japonica* under different forms of N. A, AN, and N represent the sole NH_4^+ supply, mixed N supply, and sole NO_3^- supply, respectively. The inset figures showed the anatomical limitations of g_m and the share of the overall g_m limitation by gas-phase and liquid-phase. Different letters indicate statistically significant differences ($P < 0.05$).

Figure 5. Correlations of mesophyll conductance (g_m) with the intercellular air space (f_{ias}) **(a)**, the volume fraction of cell wall thickness (T_{cw}) **(b),** the chloroplast

surface area exposed to intercellular air space per leaf area (S_c/S) **(c)**, and mesophyll thickness (T_{mes}) **(d)**. A, AN, and N represent the sole NH_4^+ supply, mixed N supply, and sole NO_3^- supply, respectively, corresponding to the symbol of the open triangles, the closed circles, and the open square in the plot. The data of each group was fitted by linear regressions ($P < 0.01$).

Figure 6. A schematic model of *L. Japonica* leaf anatomical traits and CO_2 diffusion pathway under different forms of N supply. Leaf ultrastructure model in sole NH_4^+ supply **(a)**, mixed N supply **(b),** and sole NO_3^- supply **(c),** respectively. CO_2 diffusion pathways inside the mesophyll cells in sole NH_4^+ supply**,** mixed N supply**,** and sole NO_3^- supply, respectively **(d)**. The chloroplast surface area exposed to intercellular air space per leaf area (S_c/S) was outlined with yellow lines in (b), and the mesophyll surface area exposed to intercellular airspace per unit leaf area (S_{mes}/S) was marked with purple lines in (c). The loose arrangement of mesophyll cells as affected by sole NO_3^- supply increased the intercellular airspace and consequently up-regulated the S_c/S and S_{mes}/S **(b, c)**. Increased chloroplast density resulted in reduced distance between two adjacent chloroplasts ($D_{chl\text{-}chl}$) in sole NO_3^--fed leaves **(c)**. The red folded lines and black folded lines represent the strength of CO_2 diffusion resistance into the cell from cell wall (g_{cw}), plasma (g_{pl}), cytoplasm (g_{cyt}), envelope (g_{env}) and stroma (g_{st}), while the red folded lines indicated the values of this component differed between treatments and the black folded lines means no difference between treatments or not been measured in the study **(d)**. The blue dot represents the CO_2 concentration **(d)**. T_L, leaf thickness; W, the width of the leaf section; cw, cell wall; pl, plasm; c, chloroplast.

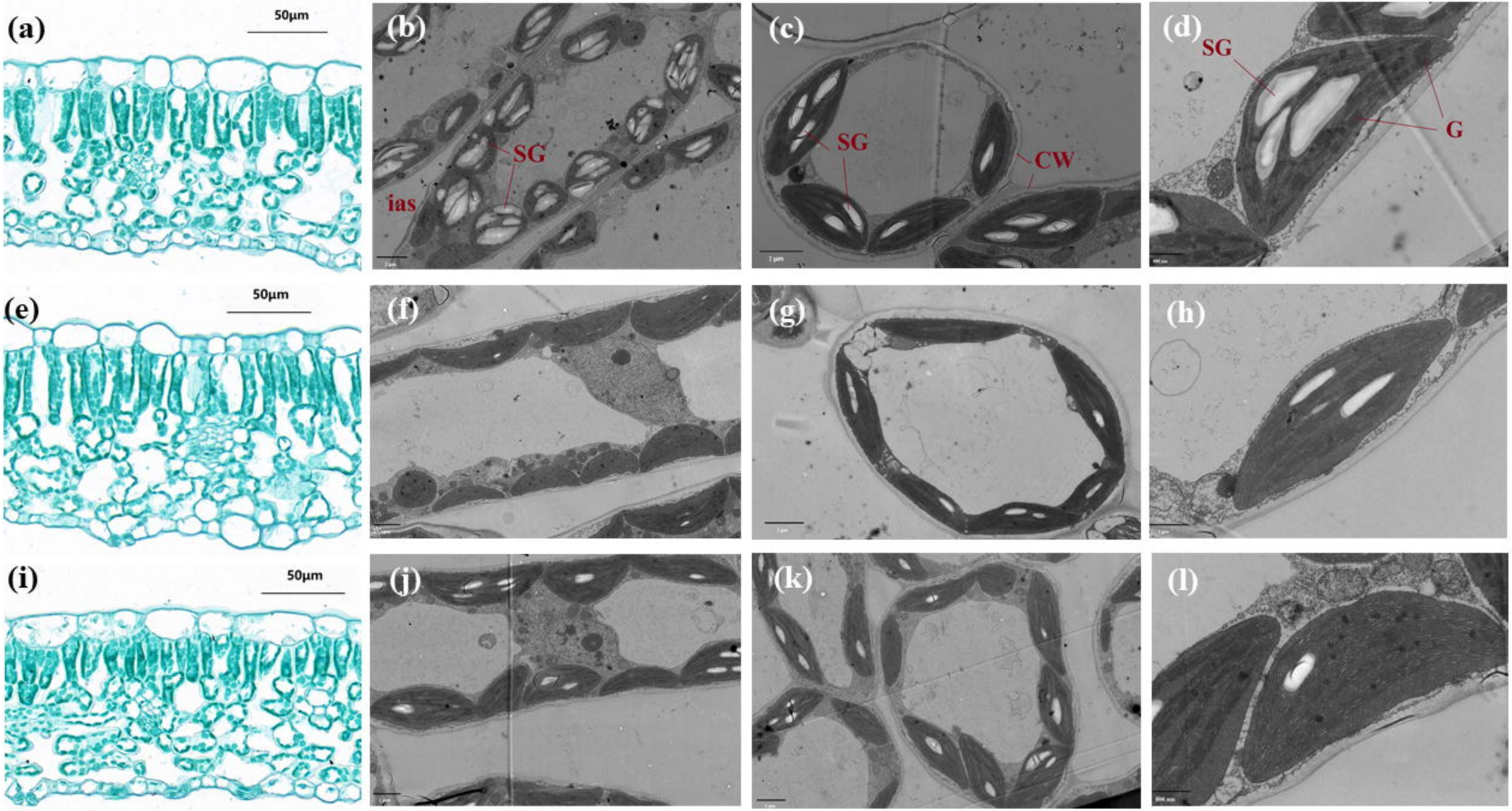
(a)
50µm
(b)
SG
ias
(c)
SG
CW
(d)
SG
G
(e)
50µm
(f)
(g)
(h)
(i)
50µm
(j)
(k)
(l)

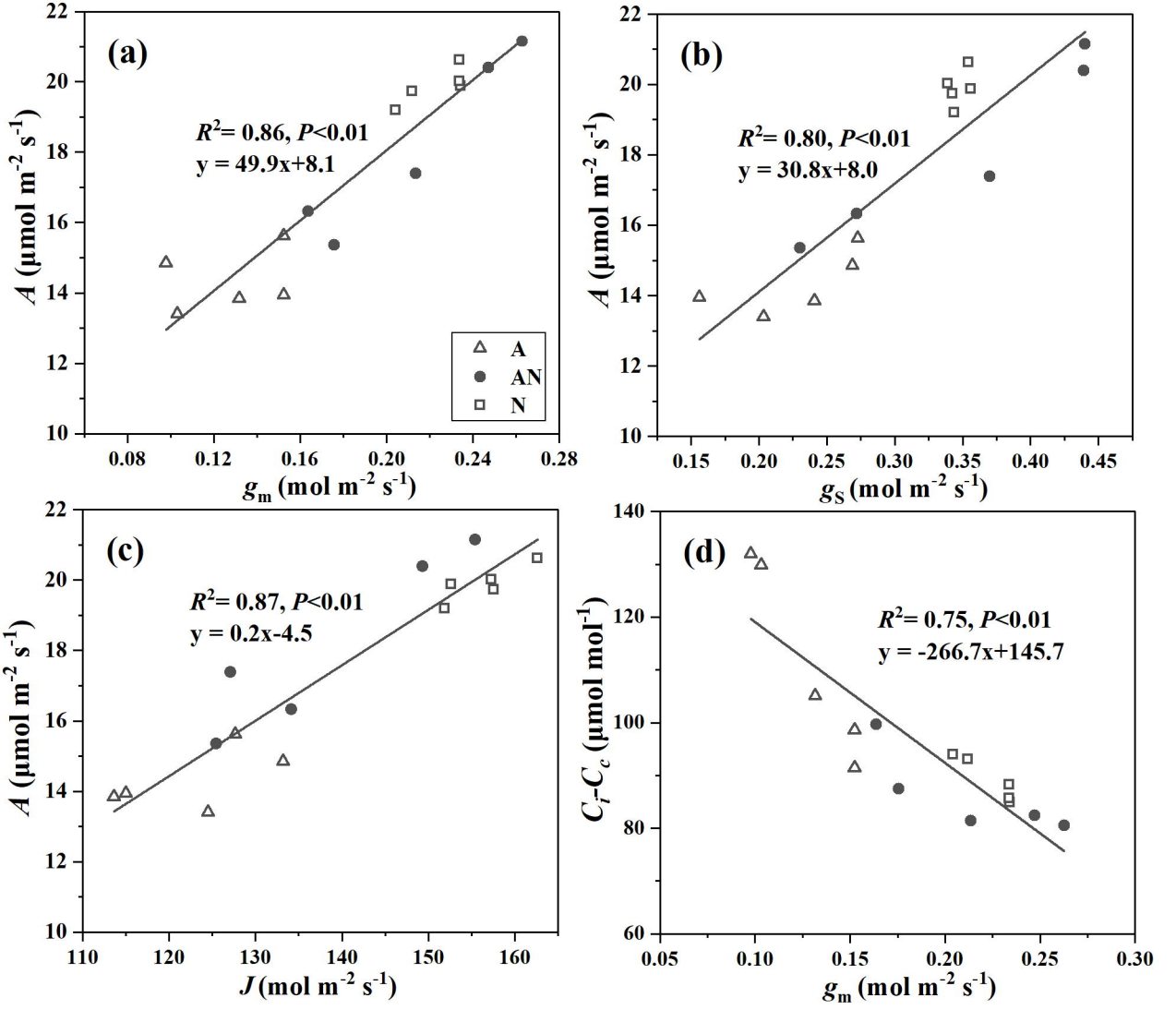
(a)
R^2= 0.86, P<0.01
y = 49.9x+8.1
A
AN
N
A (μmol m^{-2} s^{-1})
g_m (mol m^{-2} s^{-1})
(b)
R^2= 0.80, P<0.01
y = 30.8x+8.0
A (μmol m^{-2} s^{-1})
g_S (mol m^{-2} s^{-1})
(c)
R^2= 0.87, P<0.01
y = 0.2x-4.5
A (μmol m^{-2} s^{-1})
J (mol m^{-2} s^{-1})
(d)
R^2= 0.75, P<0.01
y = -266.7x+145.7
C_i-C_c (μmol mol^{-1})
g_m (mol m^{-2} s^{-1})

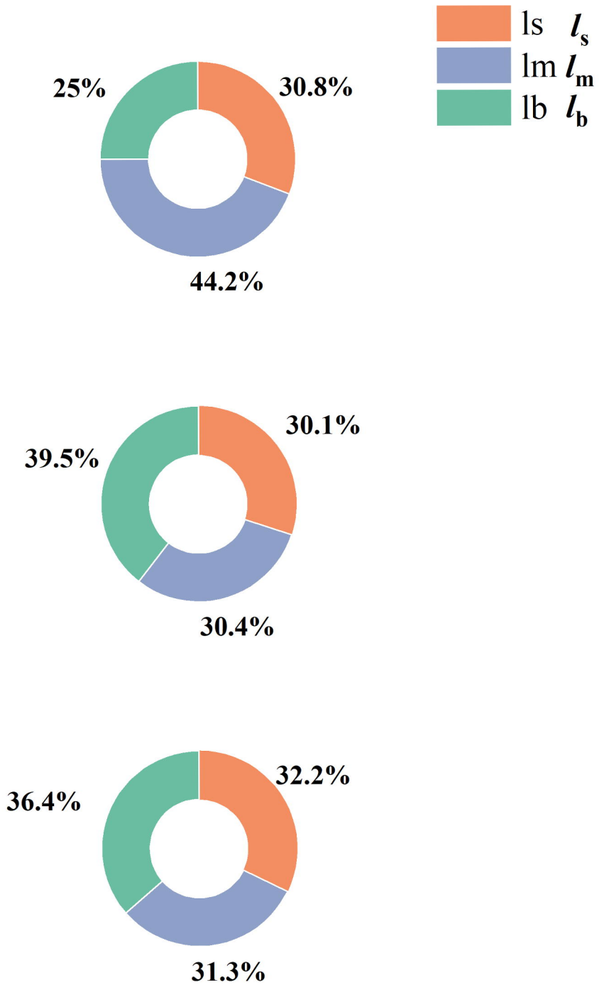
ls l_s
lm l_m
lb l_b
25%
30.8%
44.2%
39.5%
30.1%
30.4%
36.4%
32.2%
31.3%

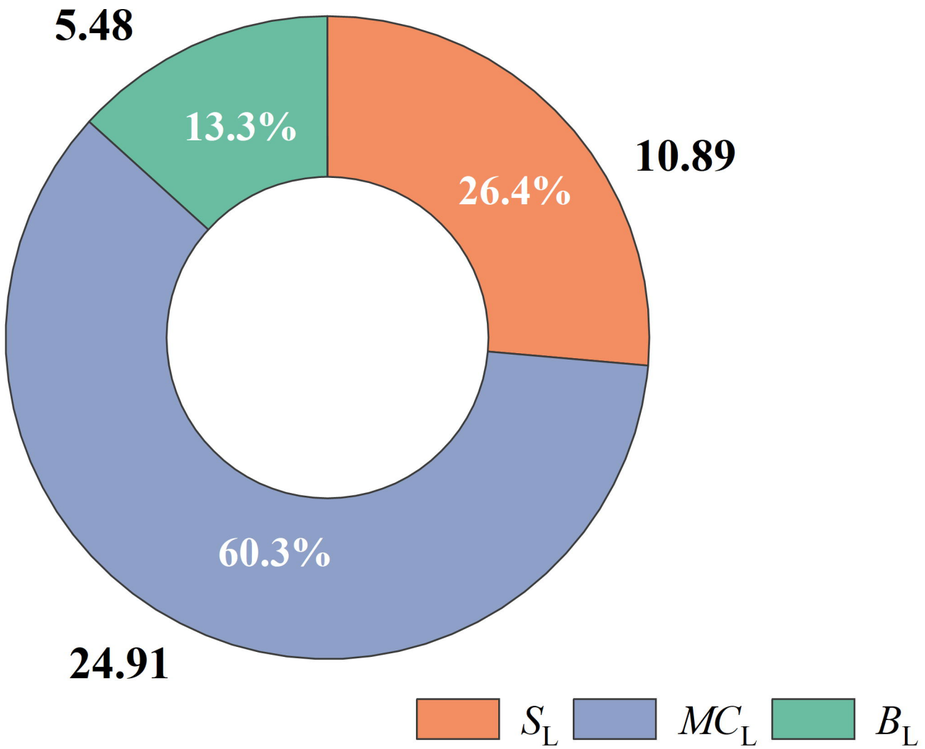
5.48
13.3%
10.89
26.4%
60.3%
24.91
S_L
MC_L
B_L

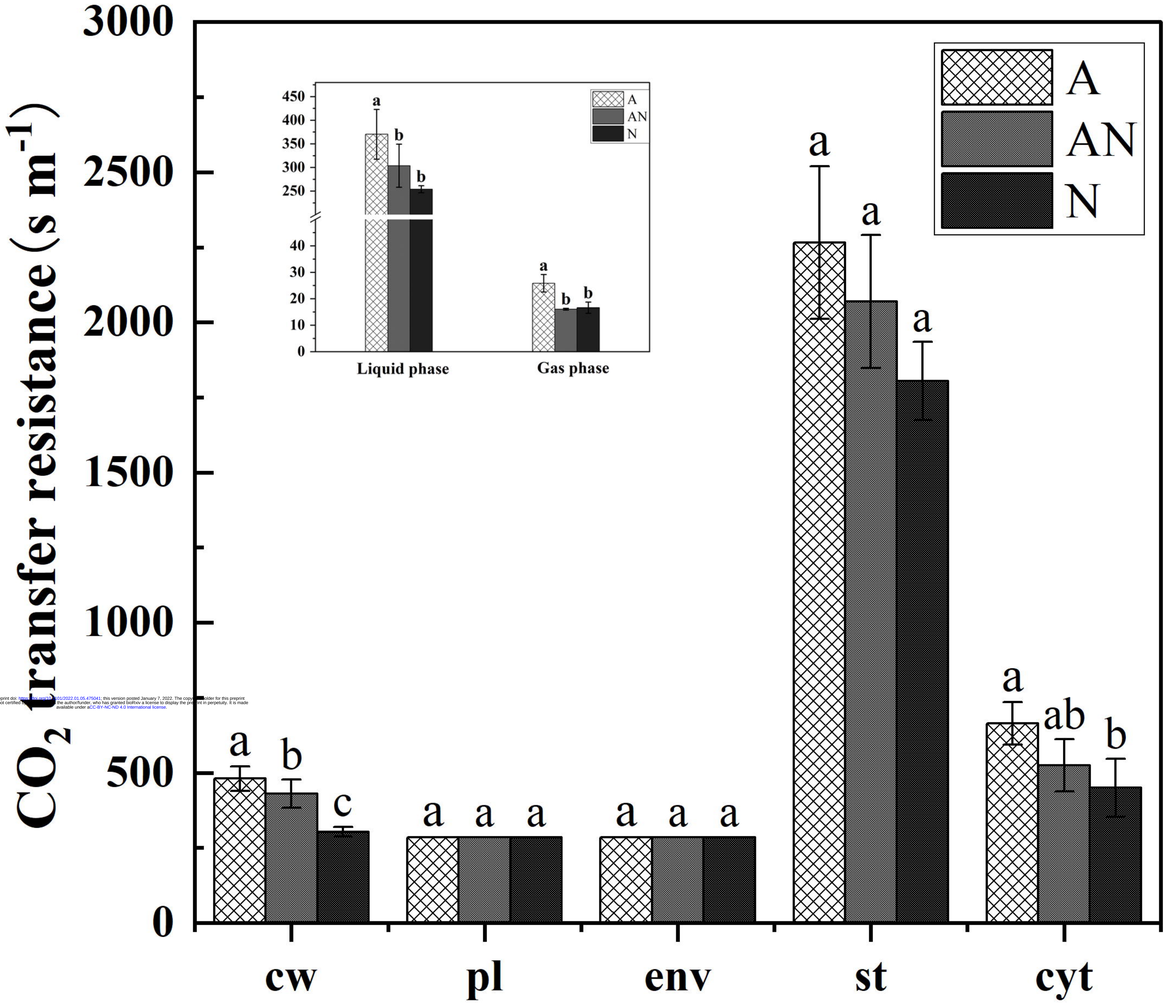

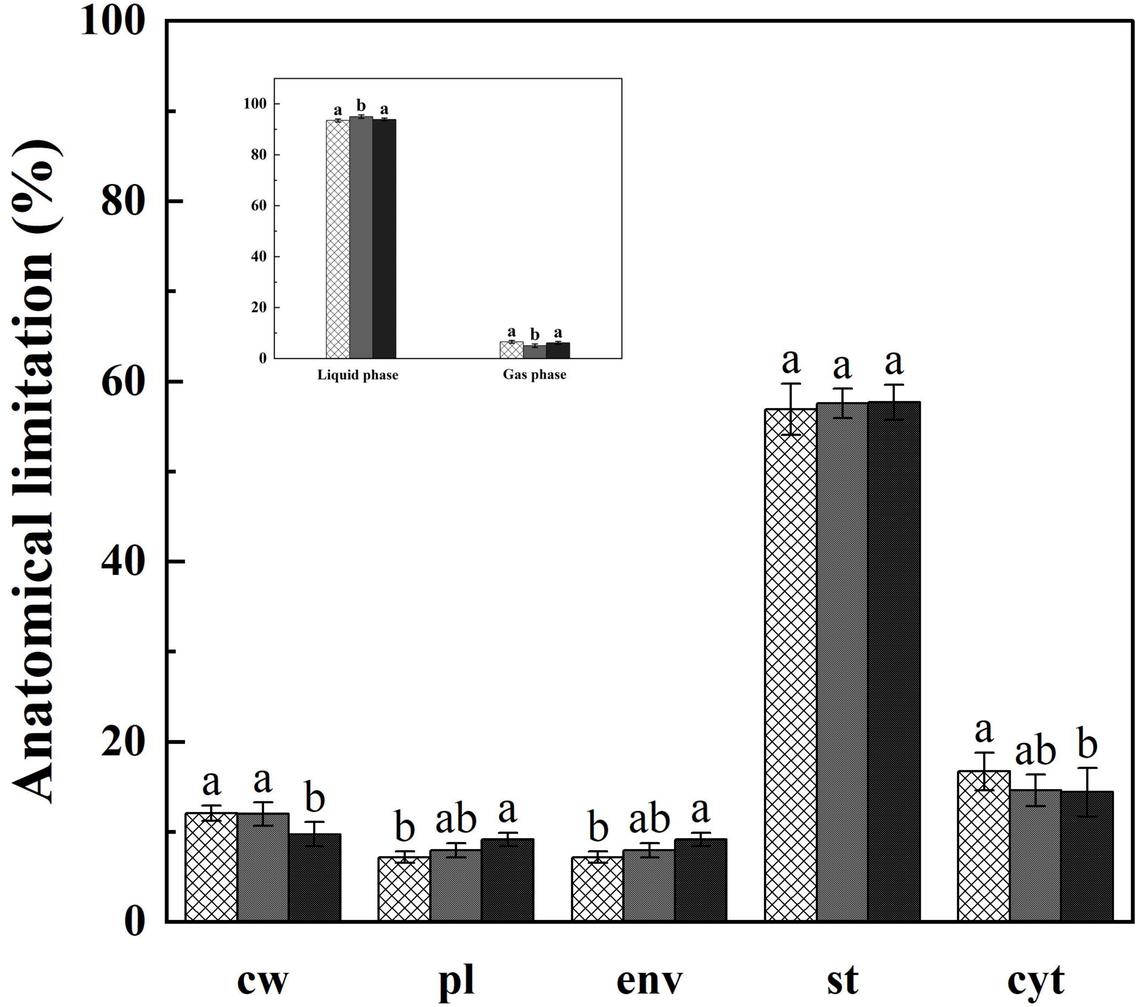

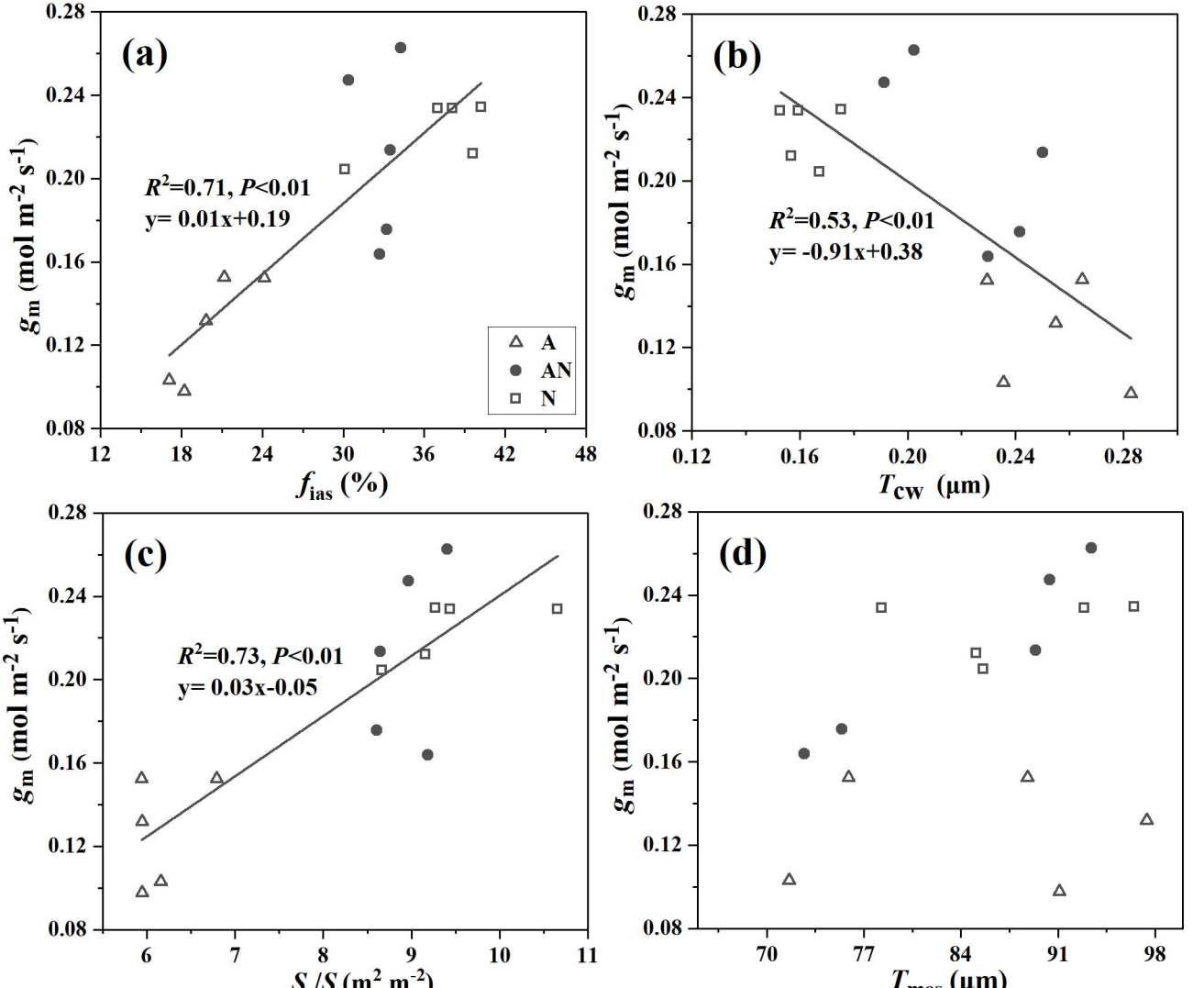
(a)
R^2=0.71, P<0.01
y= 0.01x+0.19
A
AN
N
g_m (mol m^{-2} s^{-1})
f_{ias} (%)
(b)
R^2=0.53, P<0.01
y= -0.91x+0.38
g_m (mol m^{-2} s^{-1})
T_{cw} (μm)
(c)
R^2=0.73, P<0.01
y= 0.03x-0.05
g_m (mol m^{-2} s^{-1})
S_c/S (m^2 m^{-2})
(d)
g_m (mol m^{-2} s^{-1})
T_{mes} (μm)

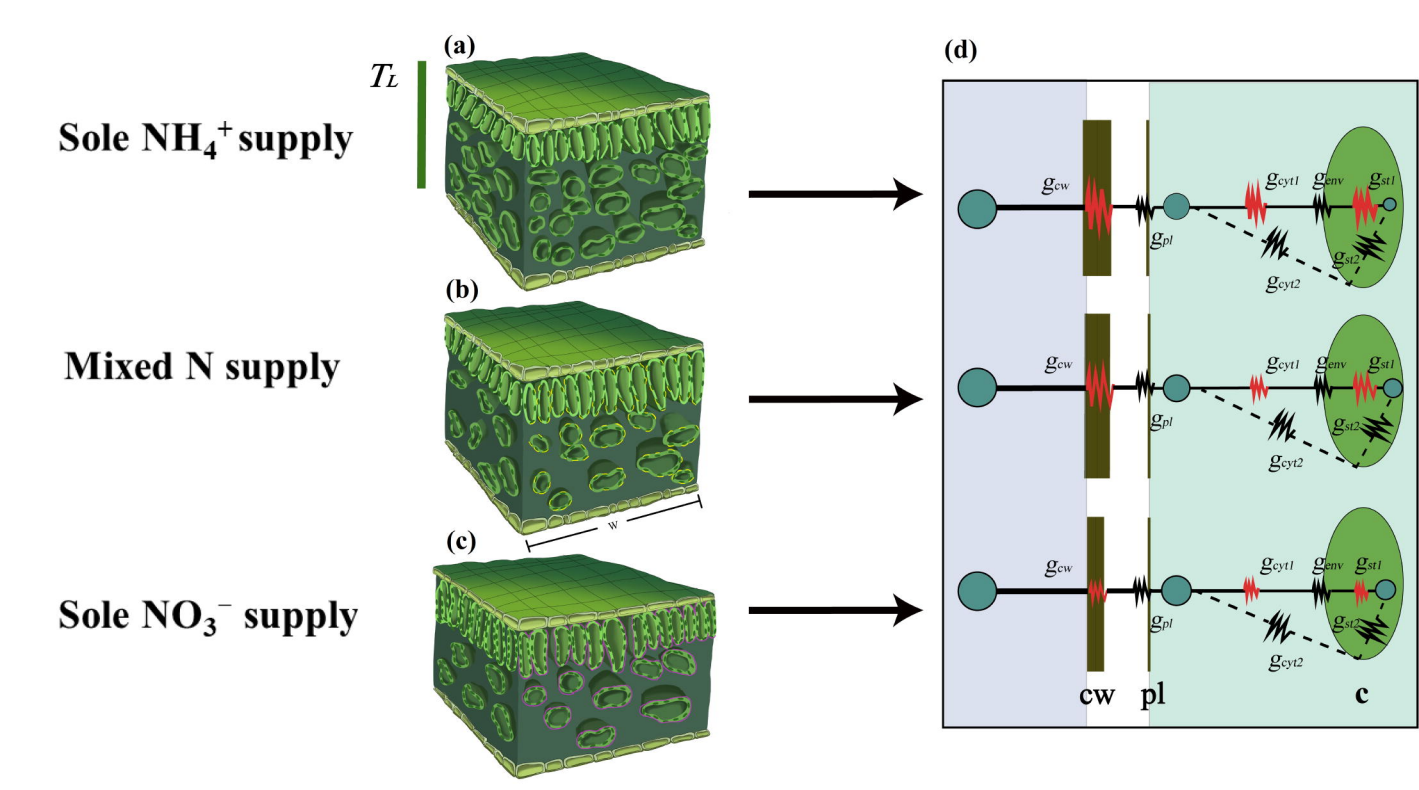
Sole NH_4^+ supply
Mixed N supply
Sole NO_3^- supply
T_L
(a)
(b)
(c)
w
(d)
g_{cw}
g_{pl}
g_{cyt1}
g_{env}
g_{st1}
g_{st2}
g_{cyt2}
cw
pl
c